

# Coincident GRB neutrino flux predictions: Implications for experimental UHE neutrino physics

Julia K. Becker <sup>a,\*</sup>, Michael Stamatikos <sup>b</sup>, Francis Halzen <sup>b</sup>  
, Wolfgang Rhode <sup>a</sup>

<sup>a</sup>*Department of Physics, Dortmund University, D-44221 Dortmund, Germany*

<sup>b</sup>*Department of Physics, University of Wisconsin, Madison, WI-53706*

---

## Abstract

In the hadronic fireball phenomenology of Gamma Ray Bursts (GRBs), it is expected that the observed photons are accompanied by UHE neutrinos, which have not been observed yet. It is one of the challenges of experimental UHE neutrino astrophysics to look for a signal from GRBs. In this paper, the differences between a search for a diffuse signal and an examination of a source sample given by e.g. BATSE will be analyzed. Since redshift information is needed to determine the correct energy spectrum, long duration bursts with redshifts from different estimate methods will be used. We will start with an overview of the current understanding of GRB neutrino physics and will then use this knowledge to make predictions for a coincidence flux and a corresponding diffuse flux. It can be shown that shape and normalization of the spectrum is highly dependent on the set of bursts used and that individual bursts can determine the total spectrum.

*Key words:* Neutrinos, GRBs, lag, variability, single source predictions

*PACS:* 95.55.Vj, 96.60.Rd, 98.62.Nx, 98.38.Fs

---



---

\* Corresponding author. Contact: julia@physik.uni-dortmund.de, phone: +49-231-7553667

## 1 Introduction

The prompt GRB photon spectrum,  $N_\gamma$ , is usually given by a Band function (1) which can be approximated by a broken power law,

$$N_\gamma \propto \begin{cases} E_\gamma^{\alpha_\gamma} & \text{for } E_\gamma < \epsilon_\gamma^b \\ E_\gamma^{\beta_\gamma} & \text{for } E_\gamma \geq \epsilon_\gamma^b. \end{cases} \quad (1)$$

The spectrum is presumably produced by synchrotron radiation of electrons in the internal shock fronts of the jet, see e.g. (2). There are two approaches to explain the break in the spectrum at a break energy of typically  $\epsilon_\gamma^b \sim 250$  keV: The most common explanation is the steepening of the spectrum by a power of one due to cooling of electrons at high energies, see for example (3; 4) as a review. The break can, however, also be explained by assuming an Inverse Compton scattering scenario, see e.g. (5) and references therein. Throughout the paper, all given energies are in the observer's frame at Earth unless declared otherwise. The spectral indices are usually scattered around average values of  $\alpha_\gamma \sim -1$  and  $\beta_\gamma \sim -2$ . Assuming hadronic acceleration in the jet, a prompt neutrino flux that is correlated to the photon spectrum results from photohadronic interactions in the source. The neutrino spectrum,  $dN_\nu/dE_\nu$ , can be derived assuming that the proton spectrum follows the electron spectrum of the source. Since the neutrino flux in turn follows the proton spectrum in first order approximation, it can thus be connected to the observed synchrotron spectrum of the sources and can be described as

$$\frac{dN_\nu}{dE_\nu} E_\nu^2 = A_\nu \cdot \begin{cases} (E_\nu/\epsilon_\nu^b)^{-\alpha_\nu} & \text{for } E_\nu < \epsilon_\nu^b \\ (E_\nu/\epsilon_\nu^b)^{-\beta_\nu} & \text{for } \epsilon_\nu^b < E_\nu \leq \epsilon_\nu^s \\ (E_\nu/\epsilon_\nu^b)^{-\beta_\nu} (E_\nu/\epsilon_\nu^s)^{-2} & E_\nu \geq \epsilon_\nu^s. \end{cases} \quad (2)$$

The photon spectral indices can be used to describe  $\alpha_\nu = \beta_\gamma + 1$  and  $\beta_\nu = \alpha_\gamma + 1$ . The second break at  $E_\nu = \epsilon_\nu^s$  in the neutrino spectrum results from the fact that pions lose energy at very high energy due to synchrotron radiation. Thus, less neutrinos result from pions at very high energies which leads to a steepening of the spectrum by a power of 2. A detailed derivation of the neutrino spectrum as presented above is given in (6).

The spectrum is normalized to the  $\gamma$ -ray fluence  $F_\gamma$  which is assumed to be proportional to the neutrino luminosity,

$$x \cdot F_\gamma = \int_{E_{\min}}^{E_{\max}} \frac{dN_\nu}{dE_\nu} dE_\nu \approx \ln(10) \cdot A_\nu. \quad (3)$$

All parameters occurring in following calculations are listed in table 1. The factor  $x$  is given by the product of the fraction of proton energy transfered to the pions,  $f_\pi$ , a factor  $1/8$  since half of the photohadronic interactions result in four neutrinos and a factor  $1/f_e$  to account for the fraction of total energy in electrons compared to protons in the jet (7). The normalization constant  $A_\nu$  is therefore given as

$$A_\nu = \frac{1}{8} \frac{1}{f_e} \frac{F_\gamma}{\ln(10)} f_\pi. \quad (4)$$

In the following, the normalization of a single burst will be modified to a quasi-diffuse normalization by multiplying  $A_\nu$  with the number of bursts per year ( $2/3 \cdot 1000$  long duration bursts per year) and dividing the result by  $4\pi$  sr,

$$A'_\nu = \frac{2}{3} \cdot \frac{1000}{\text{yr } 4\pi \text{ sr}} A_\nu. \quad (5)$$

The first break energy in the spectrum,  $\epsilon_\nu^b$ , is related to the break energy in the photon spectrum as

$$\epsilon_\nu^b = \frac{(m_\Delta^2 - m_p^2) \cdot \Gamma^2}{4 \cdot (1+z)^2} \cdot (\epsilon_\gamma^b)^{-1} \text{ GeV}. \quad (6)$$

It is determined through the minimal energy necessary to produce a  $\Delta$ -resonance in the shock fronts of the bursts. Using the numerical values given in (8) for the proton mass,  $m_p = 0.94$  GeV, and the  $\Delta$  mass,  $m_\Delta = 1.23$  GeV, leads to

$$\epsilon_\nu^b = 7 \cdot 10^5 \cdot (1+z)^{-2} \frac{\Gamma_{2.5}^2}{\epsilon_{\gamma, MeV}^b} \text{ GeV}. \quad (7)$$

The second break energy is connected to the synchrotron loss time. It depends on the neutrino flavor and for muon neutrinos, it is given as

$$\epsilon_\nu^s = \sqrt{\frac{3\pi\epsilon_e}{4\tau_\pi^0\sigma_T\epsilon_B L_\gamma}} \cdot \frac{c^4 t_v}{(1+z) \cdot m_e} \Gamma^4. \quad (8)$$

For electron and anti-muon neutrinos the break energy  $\epsilon_\nu^s$  is about an order of magnitude lower, since these neutrinos result from the muon decay. The muon lifetime is about a factor of 100 higher than the pion lifetime, which reduces the threshold of synchrotron losses. The derivation of the second break energy can be found in (7). Here,  $\epsilon_B$  and  $\epsilon_e$  are the fraction of the burst's internal energy going into the magnetic field respectively into electrons. The equipartition

fractions have been set to  $\epsilon_e = 0.1$  and  $\epsilon_b = 0.1$ . There is no good way of determining the equipartition fractions theoretically yet. However, afterglow observations indicate values of the order of 0.1 (6). The remaining parameters in Equ. (8) are listed in table 1 with the values as used in the following calculations. Inserting all numerical values gives

$$\epsilon_\nu^s = \frac{10^8}{1+z} \epsilon_e^{1/2} \epsilon_b^{-1/2} \Gamma_{2.5}^4 t_{v,-2} / \sqrt{L_\gamma^{52}} \text{GeV}. \quad (9)$$

The boost factor  $\Gamma$  is constrained to  $100 < \Gamma < 1000$ , since for boost factors less than 100, the medium would be optically thick to photons and for  $\Gamma > 1000$ , since protons lose most of their energy to synchrotron radiation. The possibility of fluctuating  $\Gamma$  using the photon break energy is given as demonstrated in (7), but there are several arguments for using a constant value: Bursts can be misaligned which would lead to a misinterpretation of the boost factor. Also, varying the break energy for each single burst might implicitly already include boost factor fluctuations. Thus, a constant boost factor of  $\Gamma = 300$  is used in following calculations.

In previous papers, e.g. (7), a variation of the fraction of energy going into pions  $f_\pi$  has been discussed. Such a variation would further increase the width of the distribution of the neutrino spectrum normalization.  $f_\pi$  varies with the burst luminosity, the boost factor, the photon break energy and the variability time as

$$f_\pi \sim 0.2 \cdot \frac{L_\gamma^{52}}{\Gamma_{2.5}^4 t_{v,-2} \epsilon_{\gamma, \text{MeV}}^b}. \quad (10)$$

In the following, this fraction will be kept at a constant value of  $f_\pi \sim 0.2$  for the following reasons:

- $f_\pi$  strongly depends on the boost factor  $\Gamma$  which will be used as a constant as discussed before. The dependence on the other three parameters is only linearly and thus not as striking as a variation of  $\Gamma$  would be.
- The main uncertainties in the current calculations result from the lack of knowledge of the parameters  $\epsilon_e$  and  $\epsilon_B$  as well as from uncertainties in the redshift relation which leads to uncertainties in  $L_\gamma$ . These three parameters are all important in the determination of the spectrum normalization and thus, a constant value is favorable.

The variability time appears in Equ. (9) as well. Apart from the arguments mentioned for the normalization of the spectrum already, the effect of varying  $t_v$  here would not be very significant in the detection rates, because the dominant contribution seen in the detector comes from the energy region of the first break.

The diffuse neutrino flux prediction derived from the model above is given in (9), where the authors use average parameters to determine the shape of the spectrum. Cosmological evolution of the sources have been considered in that model by taking into account the redshift evolution of GRBs. It is assumed that GRBs follow Star Formation Rate, since they appear to be connected to Supernova-Ic explosions. The final result of this work will be compared to this standard flux. To do this, the diffuse Waxman-Bahcall flux has to be weighted by a factor  $2/3$ , since this work only deals with long duration bursts which make up approximately  $2/3$  of the total burst population.

A different approach to predicting the neutrino flux from GRBs is to look at each burst individually and add up the individual spectra to make a prediction of the total flux from these sources. An approach of using individual spectra as discussed by Guetta et al. (7) will be used here to get an estimate of the flux that can be expected to be observed by coincident measurements of the AMANDA<sup>1</sup> telescope. In addition, a diffuse prediction will be made, using the mean values of the parameter distributions that are given or can be derived from BATSE data.

Two different burst samples based on the determination of burst redshifts using the redshift estimators variability (568 bursts) and lag (292 bursts) will be examined in this paper. A more detailed discussion of the sample properties will be discussed in section 2.

## 2 The burst samples

Due to the necessity of detailed optical afterglow observations for the determination of GRB redshifts, there are only about 61 bursts (by Oct 2005) with observed redshifts today. A histogram of the 61 observed redshifts is presented in Fig. 1. All 61 redshifts observed until today are shown as the solid line, the dashed line represents the sample of GRBs with redshift until June 2000, the BATSE era. Because of the low statistics of bursts with directly observed redshifts, different redshift estimators have been developed. Note that these methods apply only to *long duration bursts*. Although first measurements of a short duration burst redshifts succeeded recently, see e.g. (10; 11; 12), there is not enough statistics for short bursts yet. Two burst samples will be used in the following using different estimator methods for the redshift determination. Both burst sets are subsamples of the BATSE catalog:

A subsample of 568 bursts with redshifts determined using the variability of GRBs to estimate redshifts is given by Guetta et al. (7). Throughout the paper,

---

<sup>1</sup> Antarctic Muon And Neutrino Detector Array

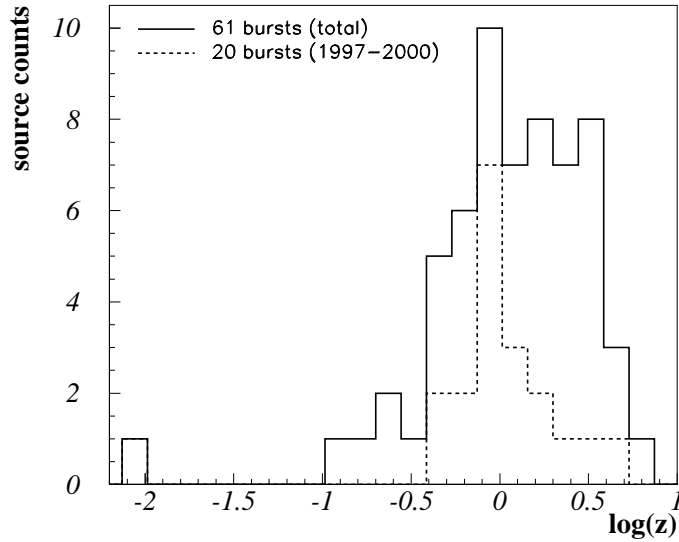


Fig. 1. Redshift distribution of 61 GRBs with measured redshifts (1997-Oct 2005, solid line). During the operation of BATSE (<June 2000), 20 bursts (dashed line) have been assigned redshifts.

it will be referred to the *variability sample* when this set of bursts is discussed. Additionally, a sample of 292 bursts with redshifts determined connecting temporal lag between the signal in BATSE’s different energy channels is given by (13), based on the work (14) and (15). Band fits have been applied to fit these spectra. We will refer to this set of GRBs as the *lag sample*.

The possibility of analyzing bursts with respect to their neutrino signal is only given for a small set of bursts because of constraints from the running UHE neutrino experiments. During BATSE’s operation time, the AMANDA experiment is one of the most interesting detectors for GRB analysis: There are 105 bursts in the BATSE catalog that can potentially be examined using the AMANDA experiment now integrated into the IceCube detector as it is pointed out in (16). None of these bursts is given in the lag sample. There are however 82 bursts of the variability sample which are in the set of the 105 bursts as well. These bursts will be discussed separately in this section. In the following, we will refer to these bursts as the *AMANDA subsample* for simplicity. A work particularly dedicated to these about 100 of these bursts will be presented soon in the context of the analysis of a potential neutrino signal from these bursts (17). Not all of the 105 bursts can actually be used for an analysis due to the restricted availability of data on either AMANDA’s or Batse’s side. A pioneer analysis of a potential neutrino signal from monster burst GRB030329 in AMANDA is described in (18).

In this section, the parameter distributions will be discussed. Each individual set of bursts will be used in section 3 to make a prediction of the flux from

the given source sample. Additionally, average values will be determined by calculating the weighted mean value of each distribution as

$$\bar{p} = \frac{\sum_{i=1}^n w(p_i) \cdot p_i}{\sum_{i=1}^n w(p_i)} \quad (11)$$

with  $1\sigma$  errors,

$$\sigma(p) = (\bar{p})^2 - \overline{p^2} \quad (12)$$

Here,  $p_i$  is the corresponding parameter value of a certain bin  $i$  and  $w(p_i)$  is the number of entries in that bin.  $n$  is the total number of bins. In each of the following parameter distributions, the average values are indicated as vertical lines. The horizontal lines show the  $1\sigma$  deviation from the average. The set of average parameters of each sample are summarized in table 2.

It should be noted that fit parameters as the spectral indices of the photon spectra,  $\alpha_\gamma$  and  $\beta_\gamma$  as well as the break energy in the photon spectrum,  $E_\gamma$ , are not identical for identical bursts in the different samples. The reason is here that the three parameters are correlated. Fixing the break energy for example at a certain energy would influence the values of the spectral indices etc.

## 2.1 Lag and Variability samples

The expected neutrino spectrum from individual bursts can be estimated from the parameters of the photon spectrum as it has been discussed in section 1. The distribution of the neutrino spectra's indices follow the one of the photon spectrum with  $\alpha_\nu = \beta_\gamma + 1$  and  $\beta_\nu = \alpha_\gamma + 1$ . The distributions of the spectral indices  $\alpha_\nu$  and  $\beta_\nu$  are displayed in Fig. 2 and 3. In all following figures, the solid line represents the distribution of the variability sample, while the dashed line shows the lag sample distribution. The distributions of the first spectral index differs between the two samples: While the lag sample shows a Gaussian behavior, the variability sample distribution does not seem to give a particular pattern. The distribution seems to be more randomly scattered. The mean values for the first spectral index are  $\bar{\alpha}_\nu^{var} = -0.89 \pm 0.44$  and  $\bar{\alpha}_\nu^{lag} = -1.62 \pm 0.56$ . The distributions of the second spectral index also show different mean values for the two samples, i.e.  $\bar{\beta}_\nu^{var} = -0.17 \pm 0.37$  and  $\bar{\beta}_\nu^{lag} = 0.63 \pm 0.62$ .

The neutrino break energies depend on the luminosity, redshift and the boost factor of the burst. The redshift distribution is displayed in Fig. 4. The variability sample has a significant contribution in the distribution at higher redshifts ( $0.8 < \log z < 1.5$ ), compared to the lag sample. Both distributions have their

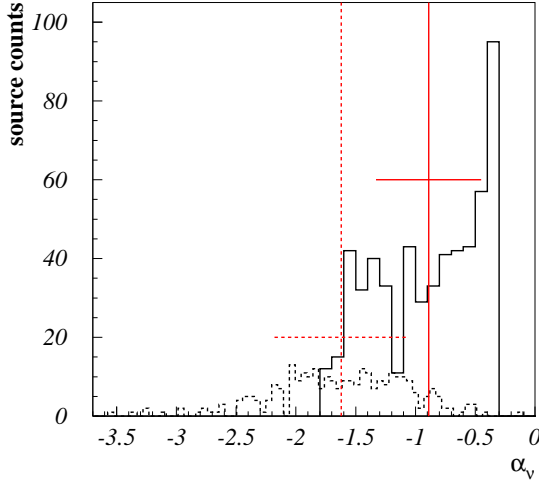


Fig. 2. Distribution of the first spectral index  $\alpha_\nu$ . Solid line: variability sample; Dashed line: lag sample. Mean values with  $1\sigma$  errors are indicated for each distribution.

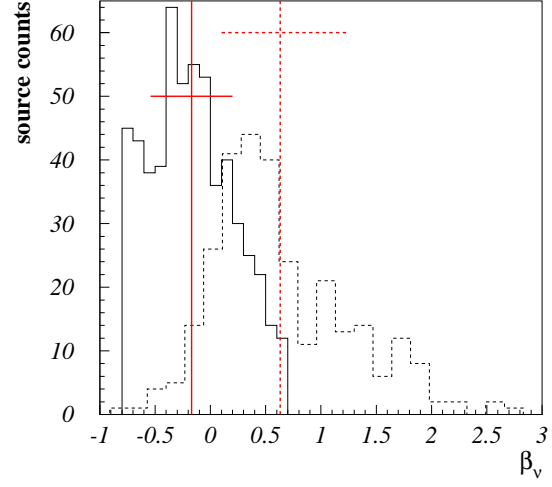


Fig. 3. Second spectral index,  $\beta_\nu$ , of the neutrino spectrum for bursts in the variability (solid line) and lag sample (dashed line). Mean values with  $1\sigma$  errors are indicated for each distribution.

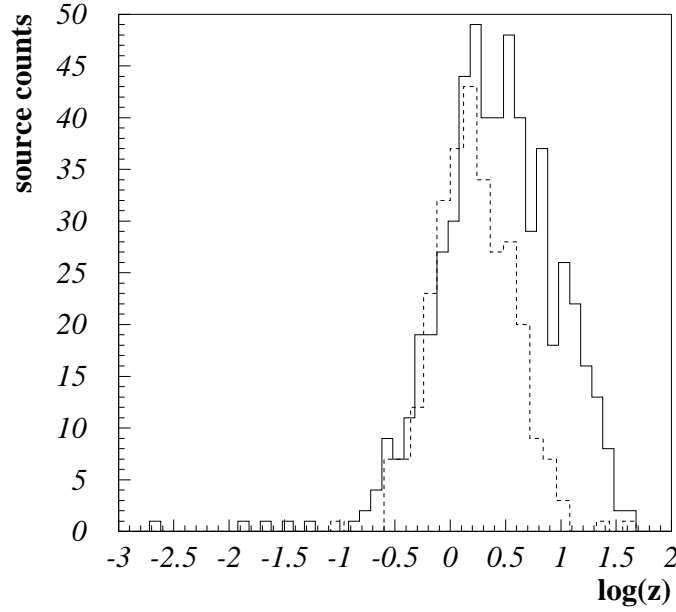


Fig. 4. Redshift distribution of the sources, solid line: variability sample; dashed line: lag sample.

maxima around  $\log z \sim 0 - 1$  which is consistent with the recent cognition that GRBs seem to follow Star Formation Rate (SFR). The boost factor is set to a constant value of  $\Gamma = 300$  as it has been discussed above.

The resulting break energies are shown in Fig. 5 and 6. Both samples scatter



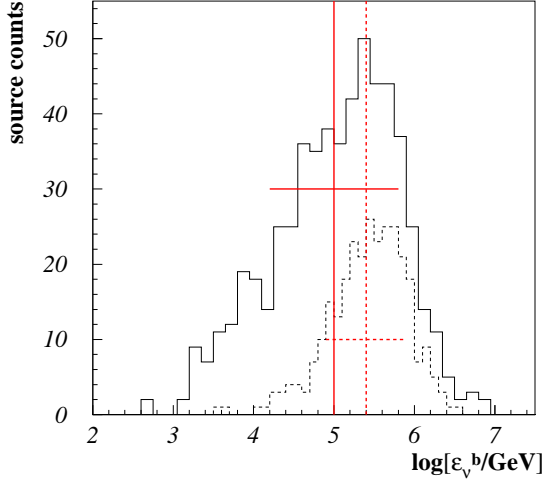


Fig. 5. Distribution of first break energy. Solid line: variability sample; Dashed line: lag sample.

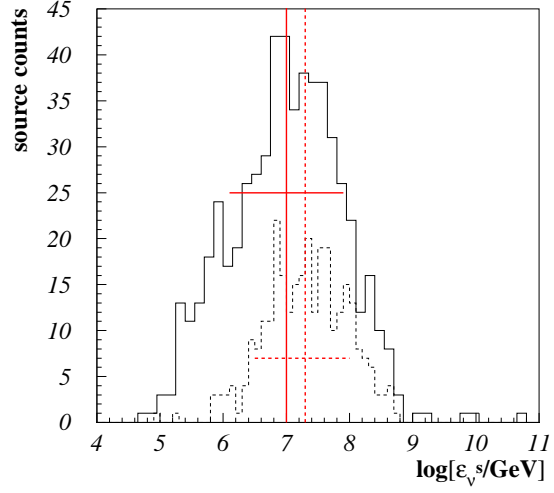


Fig. 6. Distribution of second break energy. Solid line: variability sample; Dashed line: lag sample.

widely in both break energies, so that the errors in the average values,  $\overline{\epsilon_\nu^b}^{var} = 5.0 \pm 0.8$  and  $\overline{\epsilon_\nu^b}^{lag} = 5.4 \pm 0.5$  as well as  $\overline{\epsilon_\nu^s}^{var} = 7.0 \pm 0.9$  and  $\overline{\epsilon_\nu^s}^{lag} = 7.3 \pm 0.7$  allow a deviation of about up to an order of magnitude from the mean values. Scatter plots of  $\epsilon_\nu^b$  and  $\epsilon_\nu^s$  also show that there is a relatively strong correlation between the first and the second break energy in both samples with  $\epsilon_\nu^b \propto \epsilon_\nu^s$ , see Fig. 7.

Fig. 8 shows the normalization of the variability (solid line) and lag spectra (dashed line). The distribution of the variability sample shows a peak with a mean value at  $\log[A'_\nu/\text{GeV s}^{-1} \text{ sr}^{-1} \text{ cm}^{-2}] \sim -8.8 \pm 0.6$ , while the maximum for the lag sample is slightly lower,  $\log[A'_\nu/\text{GeV s}^{-1} \text{ sr}^{-1} \text{ cm}^{-2}] \sim -9.0 \pm 0.7$ .

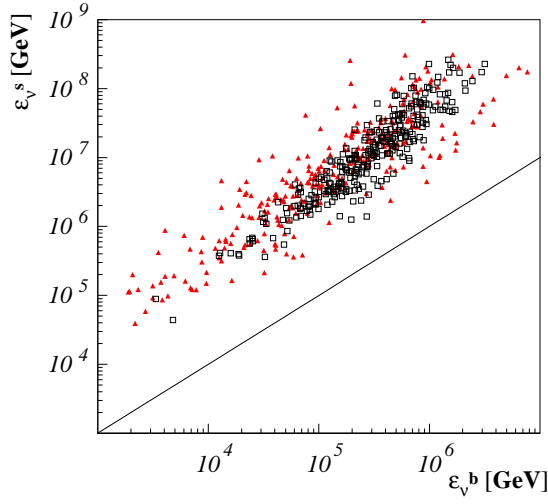


Fig. 7.  $\epsilon_\nu^b$  versus  $\epsilon_\nu^s$ . A correlation between the two break energies is present due to a correlation of Equ. 7 and 9. Black squares represent the correlation for the lag sample, red triangles represent values for the variability sample. The black line shows  $\epsilon_\nu^b = \epsilon_\nu^s$ .

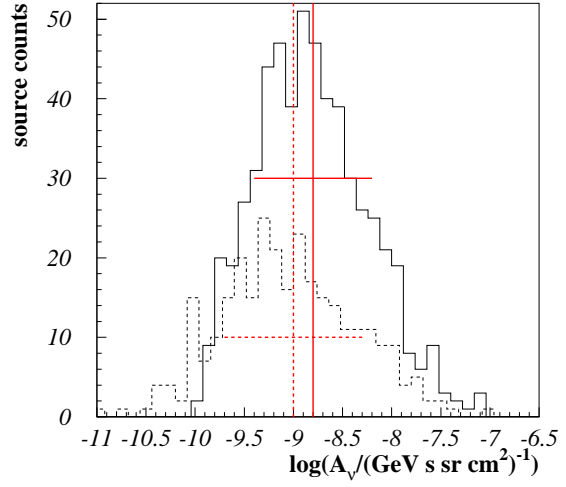


Fig. 8. Distribution of the normalization of the single burst neutrino spectra, solid line: variability sample; dashed line: lag sample.

Parameter	Symbol	Typical value
Observed photon flux	$F_\gamma$	$\sim 10^{-4} - 10^{-6}$ erg/s
Redshift	$z$	1 – 2
Luminosity distance	$d_l$	$\sim 6.5 - 15$ Gpc
Photon energy	$E_\gamma$	-
Neutrino energy	$E_\nu$	-
Equipartition fractions	$\epsilon_b$	$\sim 0.1$
	$\epsilon_e$	$\sim 0.1$
Electron-proton total energy ratio	$f_e$	$\sim 0.1$
Energy fraction transfered from $p$ to $\pi$	$f_\pi$	0.2
Burst luminosity	$L_\gamma$	$10^{52}$ erg/s
	$L_\gamma^{52} := L_\gamma / (10^{52} \text{ erg/s})$	1
Boost factor	$\Gamma$	$\sim 300$
	$\Gamma_{2.5}$	$\sim 1$
Spectral indices	$\alpha_\nu$	$\sim -1$
	$\beta_\nu$	$\sim 0$
Photon break energy	$\epsilon_\gamma^b$	$\sim 100 - 1000$ keV
	$\epsilon_{\gamma, MeV}^b := \epsilon_\gamma^b / \text{MeV}$	$\sim 0.1 - 1$
Neutrino break energies	$\epsilon_\nu^b$	$\sim (10^5 - 10^6)$ GeV
	$\epsilon_{\nu, GeV}^b := \epsilon_\nu^b / \text{GeV}$	$\sim 10^5 - 10^6$
	$\epsilon_\nu^s$	$\sim 10^7$ GeV
	$\epsilon_{\nu, GeV}^s = \epsilon_\nu^s / \text{GeV}$	$\sim 10^7$
Opening angle	$\theta$	-
Time variability	$t_v$	$\sim 10^{-3} - 1$ s
	$t_{v, -2} := t_v / (10^{-2} \text{ s})$	$\sim 0.1 - 100$
Burst duration	$t_{90}$	$\sim 2 - 1000$ s
Pion mass	$m_\pi$	140 MeV
Thompson cross section	$\sigma_T$	$0.665 \cdot 10^{-24}$ cm <sup>2</sup>
pion lifetime at rest	$\tau_\pi^0$	$2.6 \cdot 10^{-8}$ s

Table 1

Parameters for neutrinos flux calculations. The numbers quoted as "typical values" are to be taken as rough bench marks, since all of these parameters fluctuate strongly as emphasized in the text. The calculation of the luminosity distance at a redshift between  $z = 1 - 2$  is done using cosmological parameters of  $\Omega_m = 0.3$ ,  $\Omega_\Lambda = 0.7$  and  $h = 0.71$ .

	$\log [A'_\nu / (\text{GeV s}^{-1} \text{sr}^{-1} \text{cm}^{-2})]$	$\alpha_\nu$	$\beta_\nu$	$\log \epsilon_{\nu, \text{GeV}}^b$	$\log \epsilon_{\nu, \text{GeV}}^s$
variability	$-8.8 \pm 0.6$	$-0.89 \pm 0.44$	$-0.17 \pm 0.37$	$5.0 \pm 0.8$	$7.0 \pm 0.9$
lag	$-9.0 \pm 0.7$	$-1.62 \pm 0.56$	$0.63 \pm 0.62$	$5.4 \pm 0.5$	$7.3 \pm 0.7$
amanda sub.	$-8.9 \pm 0.5$	$-0.93 \pm 0.45$	$-0.24 \pm 0.37$	$4.8 \pm 0.8$	$6.8 \pm 1.0$
WB	-8.7	-1	0	5	7

Table 2

Mean neutrino spectra parameters for the three samples, variability (568 bursts), lag (292) and the variability subsample (82 bursts). The standard deviation to the mean values has been calculated as an error estimate. The values used by Waxman-Bahcall (WB) are given as reference values.

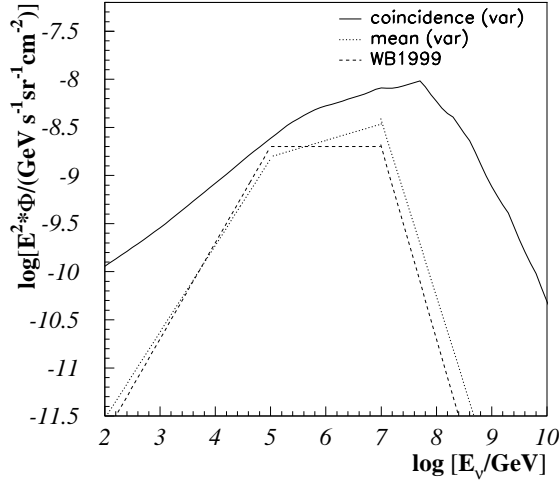


Fig. 9. Comparison of coincidence and average spectrum (variability).

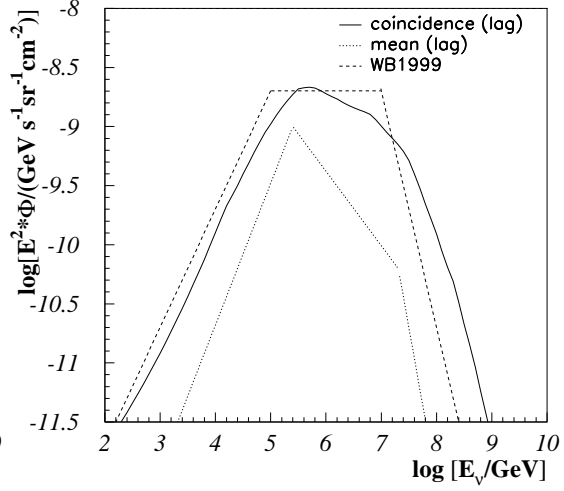


Fig. 10. Comparison of coincidence and average spectrum (lag).

The bursts that are most interesting in the presented sample in order to seek for an optimal spectrum for neutrino detection with a large volume neutrino Cherenkov telescope are those bursts with low first break energies - that means that the spectrum decreases with a relatively hard spectral index  $\alpha_\nu$  up to high energies,  $E_\nu > 10^5$ . Furthermore, high normalization bursts,  $A'_\nu > \overline{A}'_\nu$  will have a strong influence on the shape of the coincidence spectrum. The coincidence spectra are being discussed in section 3.

## 2.2 Subsample from variability for AMANDA data analysis

The last four years of BATSE operation time, 1997-2000, coincides with the beginning years of the AMANDA experiment. That implies the possibility of an examination of the neutrino signal from a BATSE subsample. 105 BATSE bursts lie within AMANDA's field of view ( $\sim$  northern hemisphere) as is examined in (16). Since the lag sample only contains bursts from before 1997, it cannot be used to examine any AMANDA burst. The variability sample however contains 82 of the 105 bursts. The parameter distributions of these bursts will not be discussed in more detail, but they are displayed in appendix A.

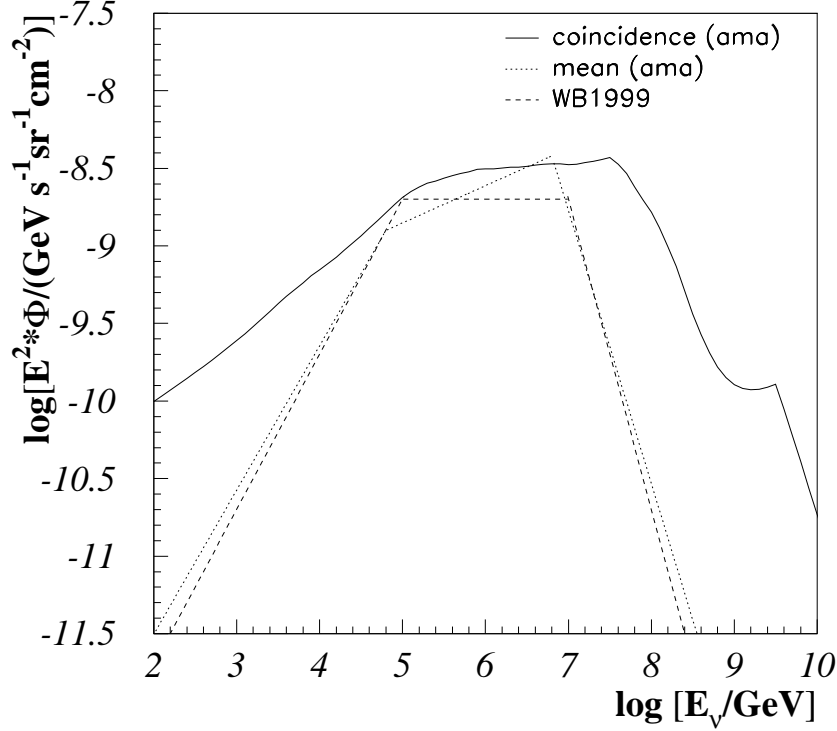


Fig. 11. Comparison of coincidence and average spectrum (AMANDA-variability subsample).

### 3 Between coincidence and average predictions

For each burst  $i$  in a sample, a prediction of the prompt neutrino flux from this source  $\Phi_i$  can be made as described above. To analyze GRBs with a large volume neutrino telescope like AMANDA, a sample of bursts is analyzed to increase the signal rate which makes it interesting to look at a coincident spectrum of burst samples. The total flux  $\Phi$  is presented in the following form in this calculation,

$$\Phi = \frac{\sum_i^n \Phi_i}{n}. \quad (13)$$

Here,  $n$  is the total number of bursts in the sample.

In this section, the coincidence spectra of each examined sample will be described in more detail. Fig. 9 shows the expected energy spectrum for the variability sample, the solid line representing the coincidence spectrum, the dotted line displaying the average spectrum calculated from the mean parameters as given in table 2. There are large differences between the two spectra, especially concerning the spectral indices at low and high energies. The differ-

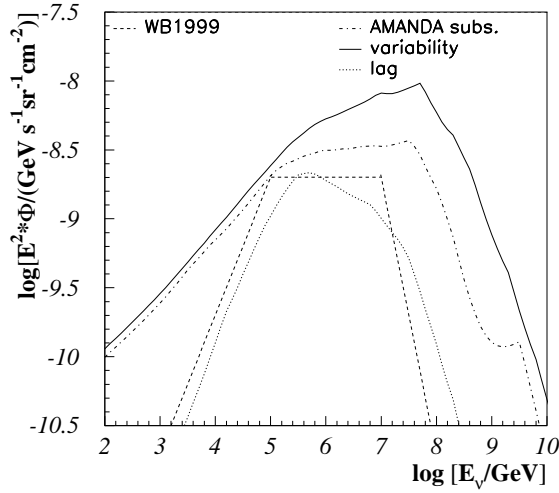


Fig. 12. 292 bursts (lag, dotted line), 568 bursts from variability method (solid line) and a subsample of 82 bursts from the variability sample which can be analyzed with AMANDA (dot-dashed line). The variability and lag sample coincidence spectra differ clearly from each other and also from the average, diffuse Waxman/Bahcall prediction. This is a strong indication that it is necessary to treat bursts individually in an analysis in order to optimize the signal expectation.

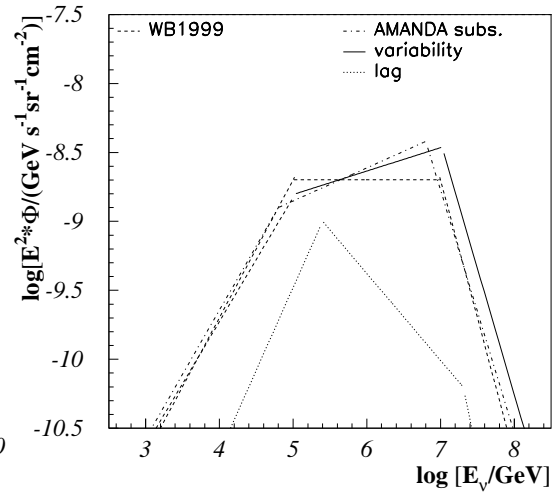


Fig. 13. Summary of the mean spectra of all samples. Major differences can be seen between the variability (solid line) and lag sample (dotted line), mostly due to differences in the second spectral index and normalization. All calculated mean spectra differ significantly from the average diffuse prediction made by Waxman and Bahcall (dashed line). The AMANDA subsample is represented by the dot-dashed line.

ences between coincidence and average spectrum in the lag sample are rather in the normalization than in the shape of the spectra, see Fig. 10. The reason for these deviations lies in the contribution of individual bursts parameters far from the average. These bursts are not considered in average calculations at all, but can be responsible for a significant change in the spectral shape and normalization. The average and coincidence flux for the AMANDA subsample is shown in Fig. 11. Both versions of the energy spectra follow the larger sample with smaller deviations, because the distributions of the subsample show a similar behavior as the whole sample (see appendix). What can also be seen is that for all samples both average and coincidence spectrum differ from the spectrum that is considered as the standard diffuse spectrum. The differences between diffuse and lag spectrum are quite small, but the spectrum of the variability sample has significantly different features compared to the diffuse spectrum.

To compare the different samples to each other, the coincidence fluxes of all samples are shown in Fig. 12. The solid line shows the variability sample spectrum and the AMANDA subsample is represented by the dot-dashed line. The lag sample is given by the dashed line. The diffuse spectrum from (9) is indicated by the dashed line as a comparison. It can be seen at first glance

that the two total samples show a very different behavior. Here, the difference from the average diffuse spectrum is of special interest, since this shows that coincidence spectra do not seem to be treatable as average diffuse spectra as easily. It can be seen that apart from the global normalization of the spectrum, the slope of especially the second spectral index is relevant for the overall normalization of the spectrum. A similar effect can be seen when comparing the average spectra of the samples to each other and to the diffuse spectrum, see Fig. 13. Here, however, the average variability spectrum agrees relatively well with the diffuse spectrum while there is quite a large difference between lag and diffuse prediction.

#### 4 Estimate of Cherenkov detection rate

An estimate of the detection rate  $R$  can be given by folding the expected neutrino flux at Earth as it has been calculated above with the probability of the detection of the neutrino,

$$R(E_{\min}, \theta) = \int_{E_{\min}} P_{\nu \rightarrow l}(E_{\nu}, E_{\min}) P_{shadow}(\theta, E_{\nu}) \Phi_{\nu} dE_{\nu}. \quad (14)$$

Here,  $P_{\nu \rightarrow l}(E_{\nu}, E_{\min})$  is the probability that a neutrino interacts with a nucleus to produce either a muon -  $l = \mu$  - or an electromagnetic cascade -  $l = \text{cascade}$  - which is detectable in a large volume neutrino detector. It can be written as

$$P_{\nu \rightarrow l} = N_A \int_{E_{\min}}^{E_{\nu}} dE_l \frac{d\sigma}{dE_l} r_l(E_l, E_{\min}) \quad (15)$$

where  $N_A$  is Avogadro's constant,  $r_l$  is the range of the produced muon -  $l = \mu$  - or cascade -  $l = \text{cascade}$  - within detection range and  $d\sigma/dE_l$  is the differential charged current cross section for  $N \nu$  interactions.  $E_{\min}$  is the energy threshold of the detector for an event detection. The cross section is determined using the parton distribution functions given by (19), where the model of (20) is used.

$P_{shadow}$  is the probability that the neutrino is absorbed by the Earth. It is given as

$$P_{shadow} = \exp(-X(\theta)/\lambda). \quad (16)$$

The neutrino absorption length  $X(\theta)$  is dependent on the angle of the incoming neutrino towards the nadir,  $\theta$ . It is determined by the distance that the



neutrino travels through Earth and the Earth's density using (21) and the atmosphere's density of the US standard atmosphere model. For a description of  $X(\theta)$  and  $\lambda$  see for example (22).

The rate of neutrino induced muons per burst is displayed in Fig. 14, the solid line representing bursts from the variability sample, the dashed line showing the bursts from the lag sample. It can be seen that there is no burst yielding the probability of a whole event in a square kilometer detection array. This indicates that a source stacking method is useful for an analysis to get a higher significance for an actual detection. Furthermore, the fits from the variability sample yields more neutrinos on average than the ones from the lag method. As it has already been stated in (7), it can be confirmed in this analysis that there are a few bursts with rates above average which will dominate the flux from the sample. Bursts below average give a small contribution to the total signal. This is demonstrated in Fig. 15: The y-axis shows the total muon neutrino rate per sample,

$$R_{tot}(R_{i_{\min}}) = \sum_{i_{\min}}^n R_i. \quad (17)$$

Here,  $i_{\min}$  is the lower summation index and  $R_i$  are the corresponding single burst rates. It is successively shifted to higher indices,  $i_{\min} = 1, 2, \dots, n$  with  $n$  as the number of sources in the sample. The sources are arranged such as the lower rates have lower indices. For instance, the lowest rate in a sample gets the index  $i = 1$ ,  $R_i$ , etc. Thus, by increasing  $i_{\min}$ , less and less sources are considered, starting by removing the least luminous ones. Fig. 15 shows  $R_{tot}$  versus  $R_{i_{\min}}$ . It can be seen that bursts with very low rates do not contribute significantly. Approaching the mean value of the distributions, however, the total rate starts to decrease rapidly. This behavior is seen in both samples. If the Waxman-Bahcall (WB) flux is used as the input spectrum (blue lines), the flux is constant at first as well, but plunges down extremely, because the rate distribution does not scatter very much as is seen in Fig. 14. The variability sample for instance shows a drop-off about an order of magnitude before the WB-flux would drop of using the same sources. At this point, the flux has already decreased by one event where all events are still captured in the WB-scenario. This one event comes from the sources below average in the variability sample - the remaining 12.7 events result from the upper part of the spectrum. This shows that most of the contribution actually comes from bursts above average. Compared to the input of real parameters, the WB-scenario would give about 4.5 events less. The lag sample in contrast would only yield 3.6 events compared to 4.7 events in the WB-scenario. Mean and total values for the different scenarios are given in table 3.

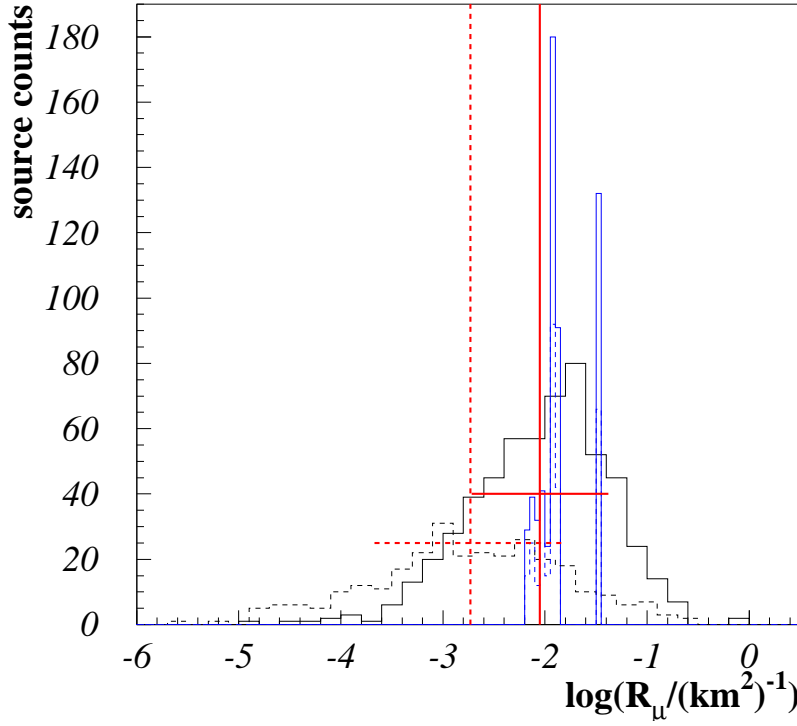


Fig. 14. Muon neutrino rates for the single bursts using a threshold energy of  $E_{\min} = 100$  GeV. The rates are given per burst and per square kilometer. On average, the neutrino flux rates determined in the lag sample are lower than the ones for the variability sample ( $\log(R_{\mu}^{\text{lag}}/\text{km}^{-2}) = -2.73 \pm 0.94$  compared to  $\log(R_{\mu}^{\text{var}}/\text{km}^{-2}) = -2.05 \pm 0.67$ ). The blue lines represent the same burst samples (solid: variability; dashed: lag) with the Waxman-Bahcall spectrum as input flux. All parameters except the angle are fixed as described above.

	mean $\nu_{\mu}$ rate [ $\text{km}^{-2}$ ]	log total $\nu_{\mu}$ rate [ $\text{km}^{-2}$ ]
variability	$10^{-2.05 \pm 0.67}$	13.8
WB [var. sample]	$10^{-1.86 \pm 0.23}$	9.12
lag	$10^{-2.73 \pm 0.94}$	3.6
WB [lag sample]	$10^{-1.86 \pm 0.23}$	4.7
AMANDA subsample	$10^{-2.05 \pm 0.59}$	1.54

Table 3

Mean neutrino spectra parameters for the three samples, variability (568 bursts, single burst parameters and WB), lag (292, single burst parameters and WB) and the variability subsample of AMANDA bursts (82 bursts). The standard deviation to the mean values has been calculated as an error estimate.

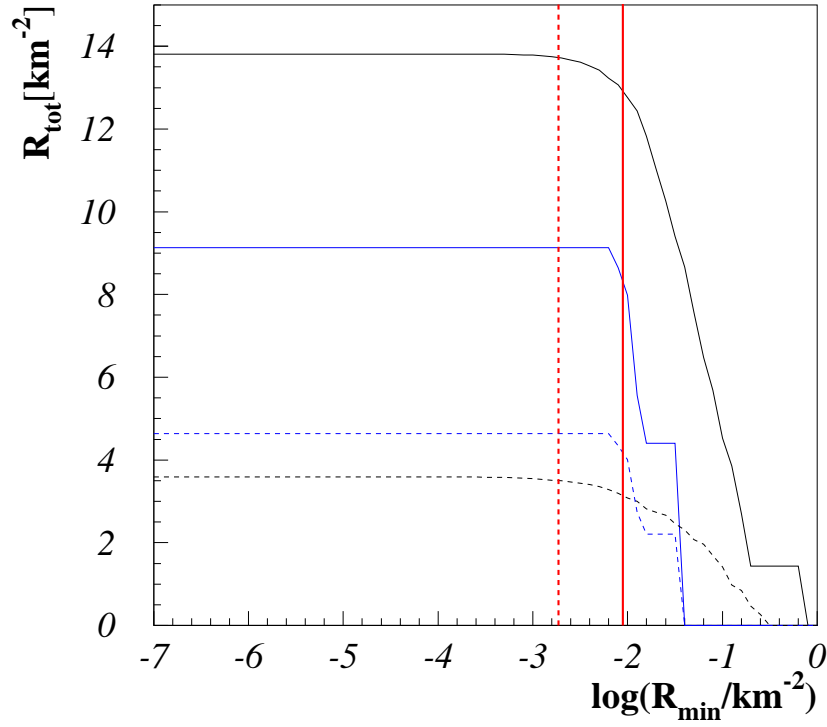


Fig. 15. Total muon rate of the complete sample (variability: solid black line, lag: dashed black line). The lower summation limit is plotted on the x-axis. Only a few sources below average (red lines) contribute to the rate. As a comparison, the samples have been regarded using the Waxman-Bahcall spectrum as an input flux (blue lines), solid: variability; dashed: lag.

## 5 Conclusions and Outlook

It is known since the detailed analysis of BATSE energy spectra that the parameters of the Band fits are not universal, but can differ significantly with the individual bursts. This implies that also the neutrino spectra of single sources have very different appearances.

The challenging task in the future will be to get a more accurate description of the redshift estimators, since until today, the relations are still derived from a very small sample of bursts with measured redshifts. The first redshift measurements of Swift give hope to a significant enlargement of the sample of measured redshifts in the near future which makes an improvement of the redshift estimators possible. Since it is known that GRBs follow Star Formation Rate (SFR), a strong redshift evolution is expected. Therefore, the redshifts are an essential parameter in neutrino flux calculations and the currently available redshift estimators are the most accurate way of dealing with redshifts so far. Other parameters like the spectral indices can be derived directly from the burst fits and therefore only include the errors due to uncertainties in the measurement of the photon spectrum.

In this paper, a prediction of the neutrino flux from individual GRBs could be made using the model of prompt neutrino emission that has been developed by (9). We follow the ansatz of (7) by using individual parameters for each burst instead of using average parameters as it has been done by (9). It could be shown that it is quite important to look at GRB neutrino spectra individually to get an accurate description of a signal from these sources. This is of special interest for large volume neutrino telescopes as AMANDA, since an accurate description of the potential signal is necessary in order to optimize an analysis. This work shows that the use of an average spectrum for analysis purposes implies the danger of a misinterpretation of the results. Particularly, it could be shown that even the average spectra of a sample of bursts is likely to differ significantly from the diffuse prediction made by (9).

## Acknowledgments

The authors would like to thank Dan Hooper, David Band and Eli Waxman for brisk and helpful discussions.

This work has been supported by the *Deutsche Forschungsgemeinschaft* (DFG).

## A Parameter distribution of the AMANDA subsample (82 bursts)

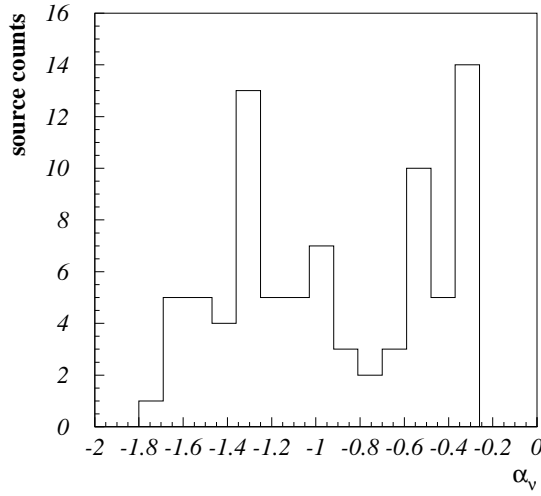


Fig. A.1.  $\alpha_\nu$ : first spectral index of the neutrino spectrum.

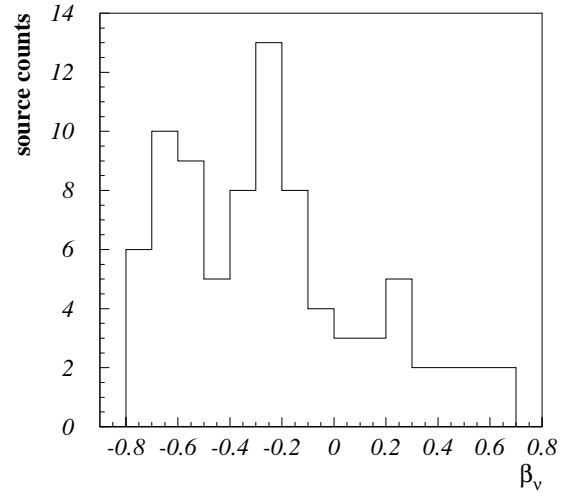


Fig. A.2.  $\beta_\nu$ : second spectral index of the neutrino spectrum.

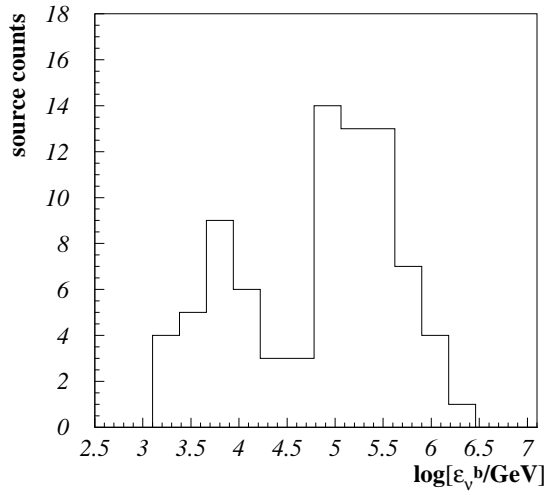


Fig. A.3. First break energy.

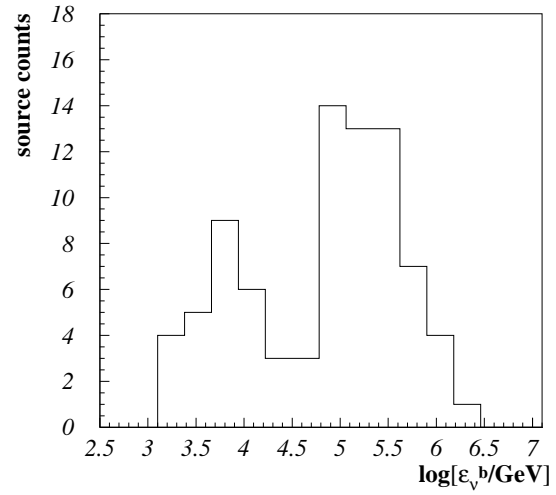


Fig. A.4. Second break energy.

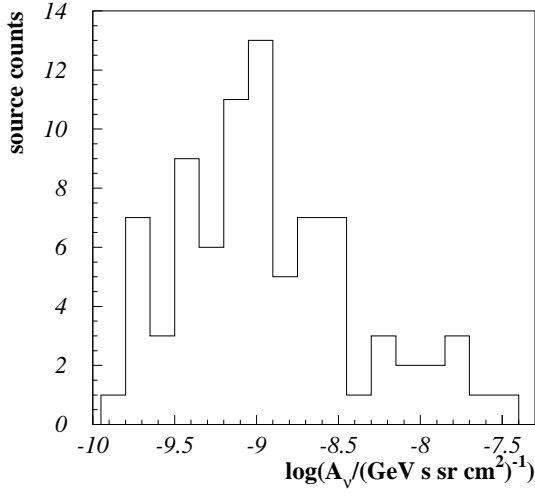


Fig. A.5. Normalization of the spectrum.

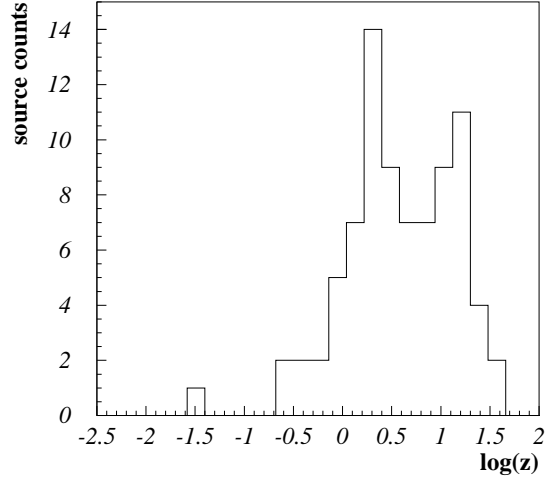


Fig. A.6. Redshift distribution.

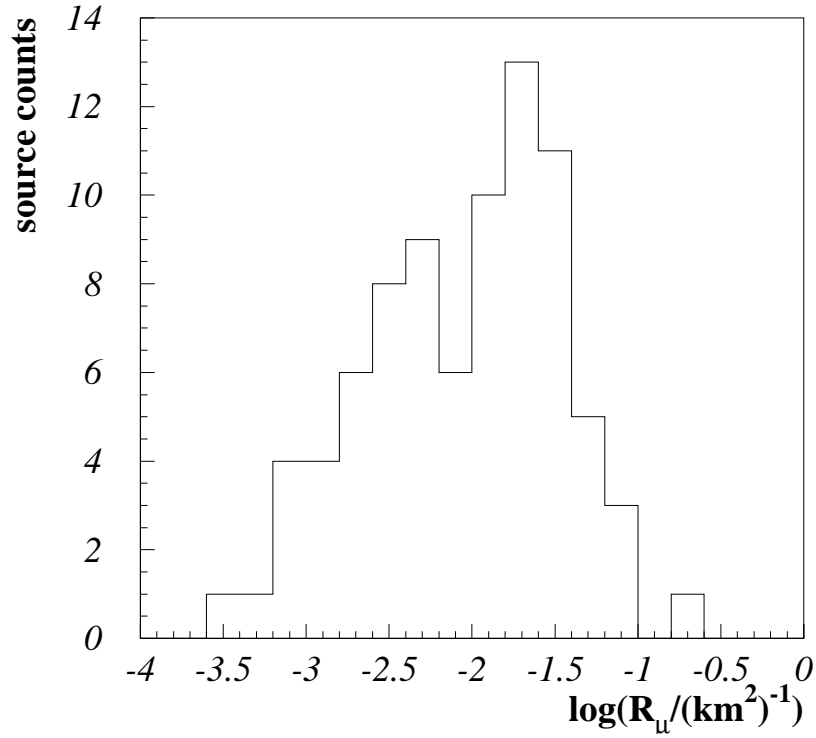


Fig. A.7. Rate distribution for the 82 bursts in the AMANDA subsample.

## References

- [1] D. Band, et al., *Astrophys. J.* 413 (1993) 281.
- [2] F. Halzen, D. Hooper, *Reports of Progress in Physics* 65 (2002) 1025.
- [3] B. Zhang, P. Meszaros, *Intern. Journ. of Modern Phys. A* 19 (2004) 2385, astro-ph/0311321.
- [4] T. Piran, *Reviews of Modern Physics* 76 (2004) 1143, astro-ph/0405503.
- [5] A. Dar, A. de Rújula, *Physics Reports* 405 (2004) 203.
- [6] E. Waxman, S. R. Kulkarni, D. A. Frail, *Astrophys. J.* 497 (1998) 288.
- [7] D. Guetta, et al., *Astroparticle Physics* 20 (2004) 429.
- [8] Particle Data Group, *Phys. Let. B* 592 (2004) 1, Particle Physics Booklet. URL <http://pdg.lbl.gov>
- [9] E. Waxman, J. Bahcall, *Phys. Rev. D* 59 (1999) 23002.
- [10] J. Hjorth, et al., *Astrophys. J. Let.* 630 (2005) L117.
- [11] J. S. Villasenor, et al., Discovery of the short  $\gamma$ -ray burst GRB 050709, *Nature* 437 (2005) 855.
- [12] J. Gorosabel, et al., ArXiv Astrophysics e-prints.
- [13] GSFC Lag-Luminosity Database, <http://heasarc.gsfc.nasa.gov/docs/cgro/analysis/lags/index.htm> (2005).
- [14] J. P. Norris, *Astrophys. J.* 579 (2002) 386.
- [15] J. T. Bonnell, et al., *Astrophys. J.* 490 (1997) 79.
- [16] M. Stamatikos, AMANDA Collaboration, in: *AIP Conf. Proc.* 727: Gamma-Ray Bursts: 30 Years of Discovery, 2004, p. 146.
- [17] M. Stamatikos, et al., In Prep. (2005).
- [18] M. Stamatikos, et al., International Conference of Cosmic Rays, Pune (India), astro-ph/0510336 (2005).
- [19] CERN, PDFLIB - User's Manual, 8th Edition.
- [20] M. Glück, E. Reya, A. Vogt, *Z. Phys. C* (53).
- [21] A. M. Dziewonski, D. L. Andersson, *Physics of the Earth and Planetary Interiors* 25 (4) (1981) 297.
- [22] T. K. Gaisser, *Cosmic Rays and Particle Physics*, Cambridge University Press, 1990.